

NEAR WAKE WEDGE AERODYNAMIC AT LOW REYNOLDS NUMBER

Tiago Barbosa de Araújo, araujob@ita.br

Roberto da Mota Girardi, girardi@ita.br

Instituto Tecnológico de Aeronáutica, Praça Mal. do ar Eduardo Gomes, 50, Vila das Acácias - São José dos Campos - SP - Brazil

Abstract. *The two-dimensional flow over bluff bodies have been discussed in several papers in the last decades. Some of these papers put their attention in the near wake flow showing that modifying it the global parameters, such as the drag coefficient, base pressure coefficient and Strouhal number, also change. It is possible to say that a better understanding of the aerodynamic behavior of this kind of flow holds on the formation region comprehension. Because of the very low velocities and the reverse flow the hot wire anemometry use become difficult due to the uncertainty associated to the calibration at very low velocities and the fact that it cannot differentiates the velocity components. To make this velocity component separation a laser Doppler anemometer is used and the mean (u and v) and fluctuant (u_{RMS} e v_{RMS}) velocities fields are acquired for a model of wedge in the range of 0.6×10^3 e 3.0×10^3 . With these flow fields is possible to determine some of the formation region parameters and its relation with the global ones. Another important aspect of this work is the results obtained at very low Reynolds number, which there isn't an experimental result for this kind of flow.*

Keywords: *Bluff Body, Near wake, LDA.*

1. Introduction

For more than one century the flow over bluff bodies are subject of studies of engineers and scientists due to its high applicability in several researching areas. However, due to its flow complexity and lack of a theory able to describe its characteristics, the studies about bluff bodies flow are largely dependent of experimental analysis (Sousa, 1993).

Several papers have been made during this period, some bringing technological aspects, such as bluff body applications at heat exchangers (Ahlborn et al, 2002) or at fuselage aerodynamics for the aeronautical sector (Girardi et al, 2007), some brings more scientific studies, such as Roshko (1954) hodograph method for obtaining theoretical bluff body drag coefficient (C_D). Most of these papers have their attention in the near wake, or formation region. This is due to some authors who showed that interfering in this region changes other flow parameters, such as the Strouhal number (St).

In their studies some authors, such as Bearman (1965), observed that near wake flow parameters are directly related to other mean flow characteristics. After this observation, many works were done using interfering elements seeking, mainly, C_D reduction using splitter plates (Rathakrishnan, 1999). Modern active wake flow control techniques, such as synthetic jets (Glezer and Amitay, 2002), can also be used for drag reduction or lift producing.

Despite all these works done, many things are not well understood and any kind of parameters prediction is made with semi-empirical models or wind tunnel experiments. On the other hand, in the past couple decades the computational methods, such as Direct Numerical Simulation (DNS) are becoming a very powerful tool. The ITA's aerodynamics group has interesting on DNS method, but this method is still limited, by the computational effort to low Reynolds number (Re) simulations. For this reason this paper will present results for this range of Re .

The formation region presents some particularities, such as very low velocities and flow recirculation, which makes hard any measurement. Because of it, a Laser Doppler Anemometer (LDA) was chosen to measure the velocity fields presented in this paper. The LDA technique main advantage is the fact of been a non-intrusive method (Tian et al, 2007). It also does not need calibration, eliminating the uncertainties associated to calibrations, because of its intrinsic response to the flow velocity, making possible the measurements of very low velocities, and the LDA technique can differentiate each velocity component, defining the flow direction, even in reverse flow regions (Jensen, 2004), what cannot be made using a hot wire anemometer.

Finishing, this paper aims to present the mean (u and v) and fluctuating (u_{RMS} and v_{RMS}) velocities fields in the formation region, for the 15° wedge at three different Reynolds numbers, 0.6×10^3 , 1.7×10^3 and 3.0×10^3 .

2. Experimental Apparatus

The measurements were performed in a open circuit wind tunnel, where the fan is placed forward the test section, manufactured by TSI (model 8390), as we can see in Fig. 1. Its test section is square and characterized by the dimension of 101.6 millimeters. The flow velocity ranges from 1.0 m/s to 32.0 m/s and 1.2% turbulence level at maximum speed with the flow seeding presence.

The model used in this work where a wedge with 15° separation angle (see fig. 2), with 9.8% of blockage ratio. The aspect ratio of the model is equal to 10.2, which the end effects can't be neglected, but only at the mean span (Mittal,

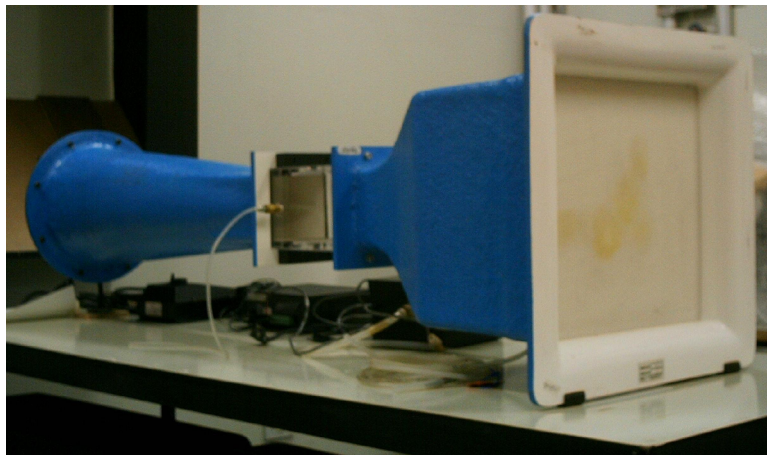


Figure 1. Wind tunnel model 8390 with square test section characterized by the dimension of 101.6 mm.

2001), where the measurements are taken.

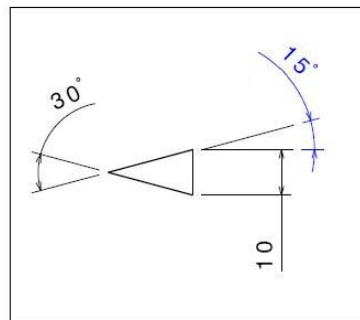


Figure 2. Lateral view of the wedge model with separation angle of 15°.

The model is placed in the test section in such a way that it stays perpendicular to the plane XOY , as shown in the fig. 3.

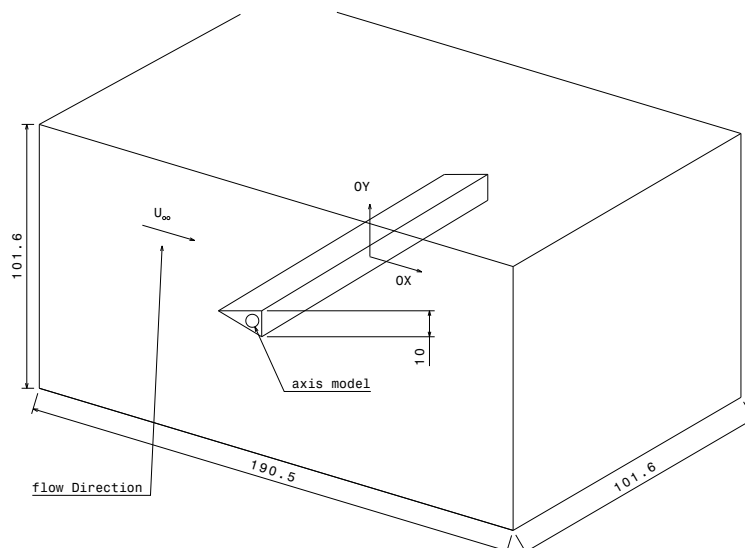


Figure 3. Test section view with a model placed at its position, with the coordinate system adopted.

To perform the flow measurements was used a LDA system equipped with an Argon-Krypton laser, using a 2D configuration. In the figure 4 is presented the system picture with its parts labeled. The LDA probe was mounted on a bench which was placed together to two-dimensional traverse with 0.1 mm precision.

The flow seeding utilized in this work was olive oil, which was atomized by a particle generator made by TSI (model 9307). This generator was calibrated to produce droplets with mean diameter of 1.0 μm which are suitable for low Mach

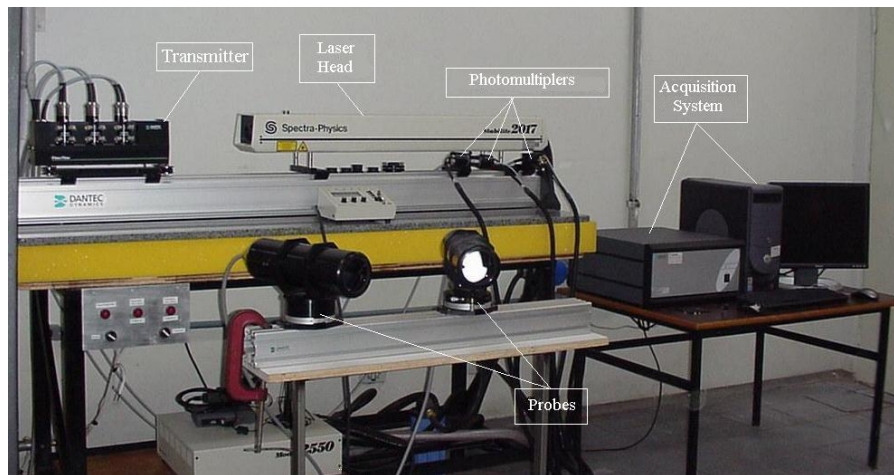


Figure 4. General view of the LDA setup.

number regimes and for turbulent flow with 10 *KHz* maximum frequency (Melling, 1997). The dynamic pressure was controlled by a WIKA (Tronic Line) micromanometer which ranges from 0.0 *mbar* to 1.0 *mbar* (100,0 *Pa*). This was calibrated from 0.0 *m/s* to 12.0 *m/s*. For more detailed description of this experimental apparatus can be seen in Araújo and Girardi (2009a).

3. Experimental Procedure

Considering the model set in the wind tunnel section, as shown in the figure 3, and aligned with the flow direction (see Araújo and Girardi, 2009a). We have to ensure that the measurement volume is placed at model middle-span and the wind tunnel is well aligned to the *LDA* coordinate system (see Araújo and Girardi, 2009b). Then, with the measurement time defined (see Araújo and Girardi, 2008) to the flow in the wake and outside it, 64 seconds and 32 seconds respectively, we can measure the velocity profiles, as explained below. The measurement time difference between the velocities taken in the wake and out it is due the flow characteristic. In the inner measurements the measurement volume is subject to vortex passage, this makes the fluctuant velocity larger than outside the wake, requiring larger time to get good averages.

With the origin set at the middle-span and half base length (*d*), we can define the coordinate system as: the *y*-direction is the direction parallel to the base model pointing to the wind tunnel upper surface, the *x*-direction is the freestream direction and the *z* direction is the span direction. The profiles measurements are taken in the plane *XOY* keeping the *z*-direction constant.

Taken after the precautions, cited in the papers at the previous paragraphs, we measure the velocity profiles at *y*-direction. The profile is started at $y = 0.2d$ and goes until $y = 1.2d$ by increments of $0.1d$, except at the separation point region where the mesh is refined and the increments are of $0.05d$. This refinement is made to better define the velocity profile in the free shear layer.

Finishing the profile measurement, the traverse system is moved on the *x*-direction by the increment of $0.1d$ and a new profile is taken, repeating the above procedure. The increments on the *x*-direction are kept constant from the origin to $2.0d$, after it becomes $0.2d$ until the measurement volume reaches $3.0d$. The procedure describe in the two previous paragraph is repeated until all the measurements are taken.

4. Results

This section is devoted to present the flow fields obtained from the *LDA* measurements for the three Reynolds number, cited before. The fields here presented were obtained keeping the blockage, aspect ratio, separation angle constants, to the flow direction aligned model. In the figure 5 are presented the non-dimensional vorticity fields, defined by the equation 1, for the three Reynolds numbers (*Re*). In this figure is also shown the streamlines for each *Re*. The letters A, B and C represents the maximum longitudinal fluctuant velocity (u_{RMS}/U_∞) position, which by Bearman (1965) defines the formation region end, and D, E and F represent the maximum transversal fluctuant velocity (v_{RMS}/U_∞) position.

$$\omega_z = \frac{1}{2} \left(\frac{\partial v}{\partial x} - \frac{\partial u}{\partial y} \right) \quad (1)$$

First of all, we can observe in the figure 5 that the region containing the negative vorticity gets more concentrated with the Reynolds number increasing. The *Re* increasing makes the boundary layer thinner, what concentrates the released vorticity created, at the body, in smaller flow region. We cannot forget that the presented fields are time means and shows

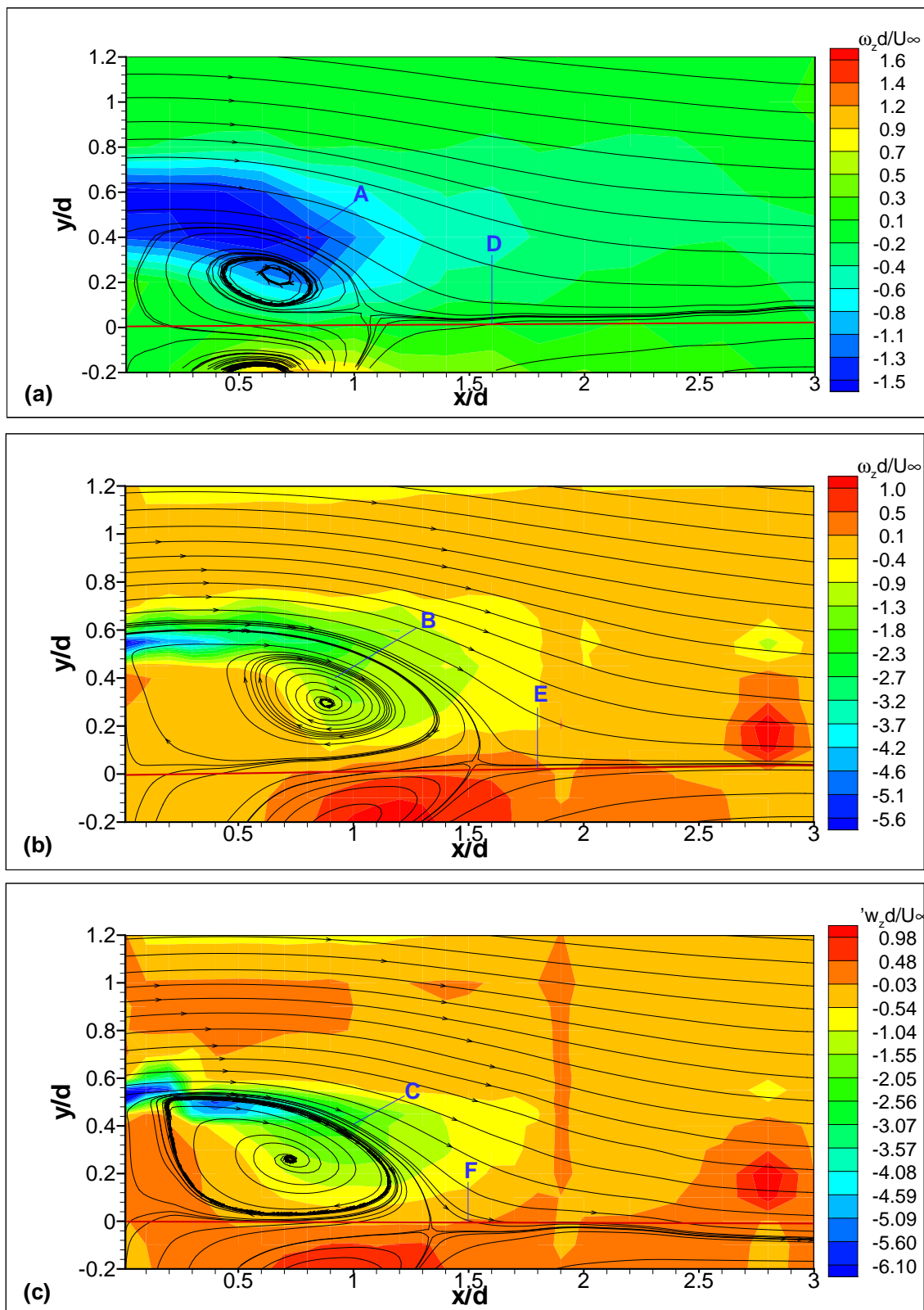


Figure 5. Non-dimensional vorticity field for the Reynolds numbers of (a) 0.6×10^3 , (b) 1.7×10^3 and (c) 3.0×10^3 , with non-dimensional uncertainty of 40%, 45% and 32%, respectively. All uncertainties with 95% of probability

the mean shear layer position, which shakes up and down from these mean positions.

We can observe from this figure that the mean vorticity minimum gets more negative with the Reynolds number increment, what is reasonable once the vorticity rate released from the body is basically due to the difference between the inner and outer free shear layer velocities at the separation point (Fage and Johansen, 1927), and these velocities increase with Re .

The increase in the mean vorticity can also be observed by the vortex strength (Γ), that can be defined by the equation 2 (obtained by integrating, in one period, the Fage and Johansen (1927) approximation) and is shown in the table 1. As we can observe directly from the figure 5, the fact that Γ increases does not mean an enlargement in the mean vortex shape. Unlike there is a reduction in its shape from the Reynolds number of 1.7×10^3 to 3.0×10^3 .

$$\frac{\Gamma}{U_{\infty}d} = \frac{K^2}{2St} \quad (2)$$

Where K and St are the base pressure parameter and the Strouhal number, respectively.

In the table 1 are presented the some flow parameters variation with the Reynolds number increasing, such as the Strouhal number (St) and the maximum u_{RMS} x-position (X_{ur}), which give us a vortex formation measurement. The (St) variation presented in this table confirm the affirmation in the previous paragraph, that the mean vortex increases in the first Re increment, but unlikely it diminishes in the second increment, despite of the vortex strength increasing.

Table 1. Parameters variation with the Reynolds number increment.

| Re | $\frac{X_N}{d}$ | $\frac{Y_N}{d}$ | $\frac{X_{ur}}{d}$ | $\frac{Y_{ur}}{d}$ | $\frac{X_{vr}}{d}$ | $\frac{l_S}{d}$ | K | C_{Pb} | St | $\frac{\Gamma}{U_{\infty}d}$ | $\frac{l_S}{X_N}$ |
|-------------------|-----------------|-----------------|--------------------|--------------------|--------------------|-----------------|-------|----------|-------|------------------------------|-------------------|
| 0.6×10^3 | 0.66 | 0.23 | 0.6 | 0.4 | 1.6 | 1.1 | 1.162 | -0.35 | 0.251 | 2.69 | 1.67 |
| 1.7×10^3 | 0.88 | 0.30 | 0.9 | 0.3 | 1.8 | 1.5 | 1.204 | -0.45 | 0.210 | 3.45 | 1.70 |
| 3.0×10^3 | 0.73 | 0.26 | 1.0 | 0.3 | 1.5 | 1.3 | 1.313 | -0.72 | 0.233 | 3.70 | 1.78 |

The base pressure coefficient (C_{pb}) values here presented were obtained from K (see eq. 3), which is the ratio between the separation velocity and the undisturbed flow velocity. Where the separation velocity is the one measured on the outer shear layer point. Its tendency of getting more negative is due to the separation velocity growing with the Reynolds number increment.

$$C_{pb} = 1 - K^2 \quad (3)$$

Despite the Reynolds number increment be almost equal the decrement in base pressure coefficient, it is larger from $Re = 1.7 \times 10^3$ to $Re = 3.0 \times 10^3$, which is accompanied by a near wake topological change. In this Re increment the mean vortex core gets closer to the body base, what can also affect this parameter, making the base pressure increment larger. It is possible because the lower vortex pressure is encountered in its core (Milne-Thomson, 1974).

In the figure 6 is shown the longitudinal (u/U_{∞}) mean velocity field for the three Reynolds numbers with its streamlines superposed. As in figure 5 the letters A, B, C, D, E and F represent the maximum fluctuant velocity position. We can see in this figure that the maximum and minimum values have not such a great changing with the Re increment.

It is also possible that the saddle point position (l_S/d) has the same behavior of the mean vortex core position, see table 1. But the ratio l_S/X_N is not constant, it grows almost linearly. However for confirming this behavior more experiments are needed for others Reynolds numbers, to see if it keeps the same fashion. The values of l_S/d in the table 1 has the uncertainty equal to 0.1 and to verify this linear tendency it is also necessary to refine the mesh in the saddle point region, decreasing its uncertainty

In the figures 7 and 8 are presented the longitudinal (u_{RMS}/U_{∞}) and transversal (v_{RMS}/U_{∞}) fluctuant velocity fields and as before the maximums RMS values are represented by letters. The peaks are not well defined, but they can be seen as a central maximum point, because the RMS values at its neighborhood is inside the measurements accuracy, which is 0.1. However for the maximum v_{RMS}/U_{∞} we can say that the tendencies are kept, for the u_{RMS}/U_{∞} , but we can not take any clear conclusion about the second Reynolds number increment.

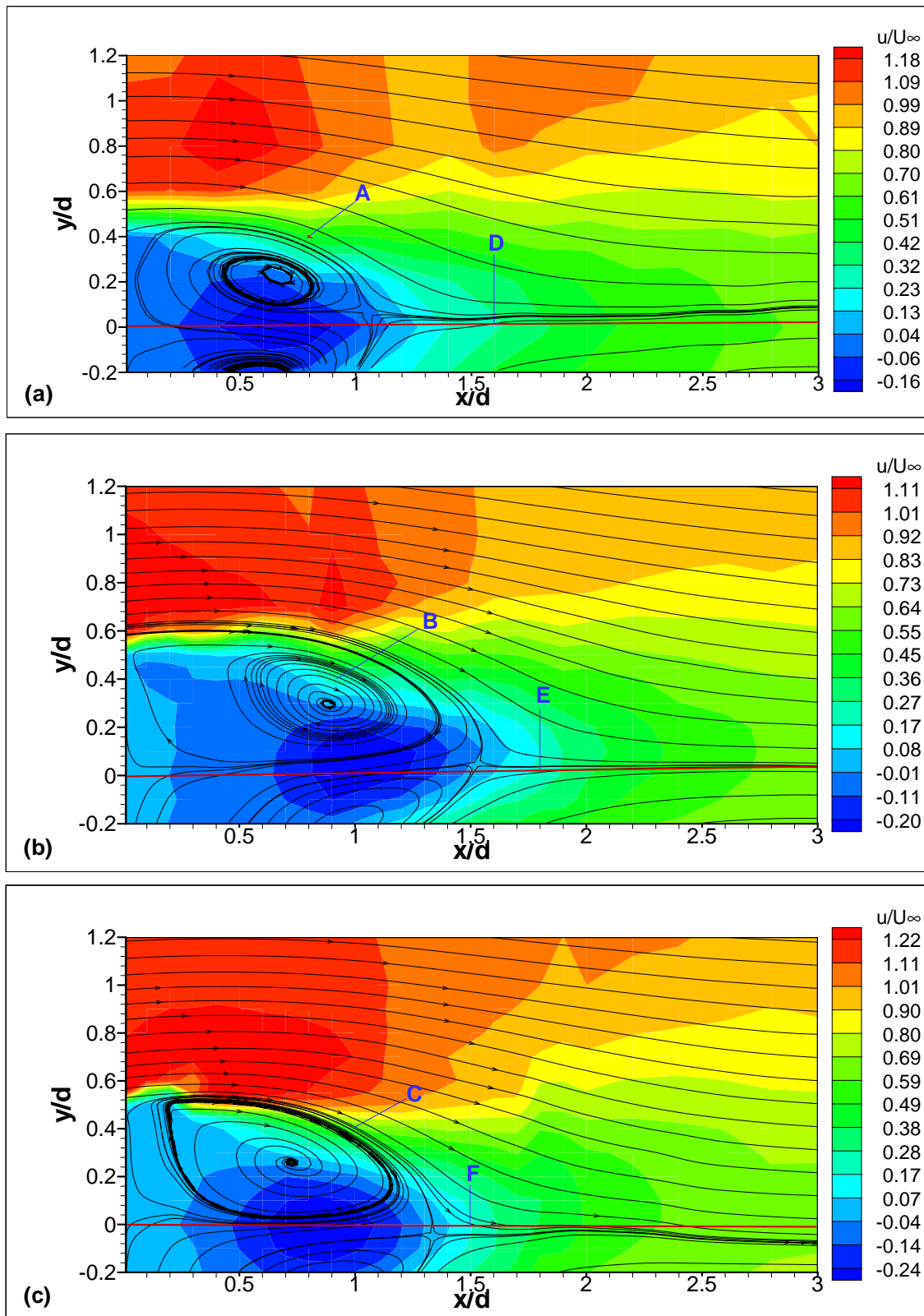


Figure 6. Longitudinal mean velocity field with stream lines for the Reynolds numbers of (a) 0.6×10^3 (non-dimensional uncertainty of ± 0.03), (b) 1.7×10^3 (non-dimensional uncertainty of ± 0.01) and (c) 3.0×10^3 (non-dimensional uncertainty of ± 0.002).

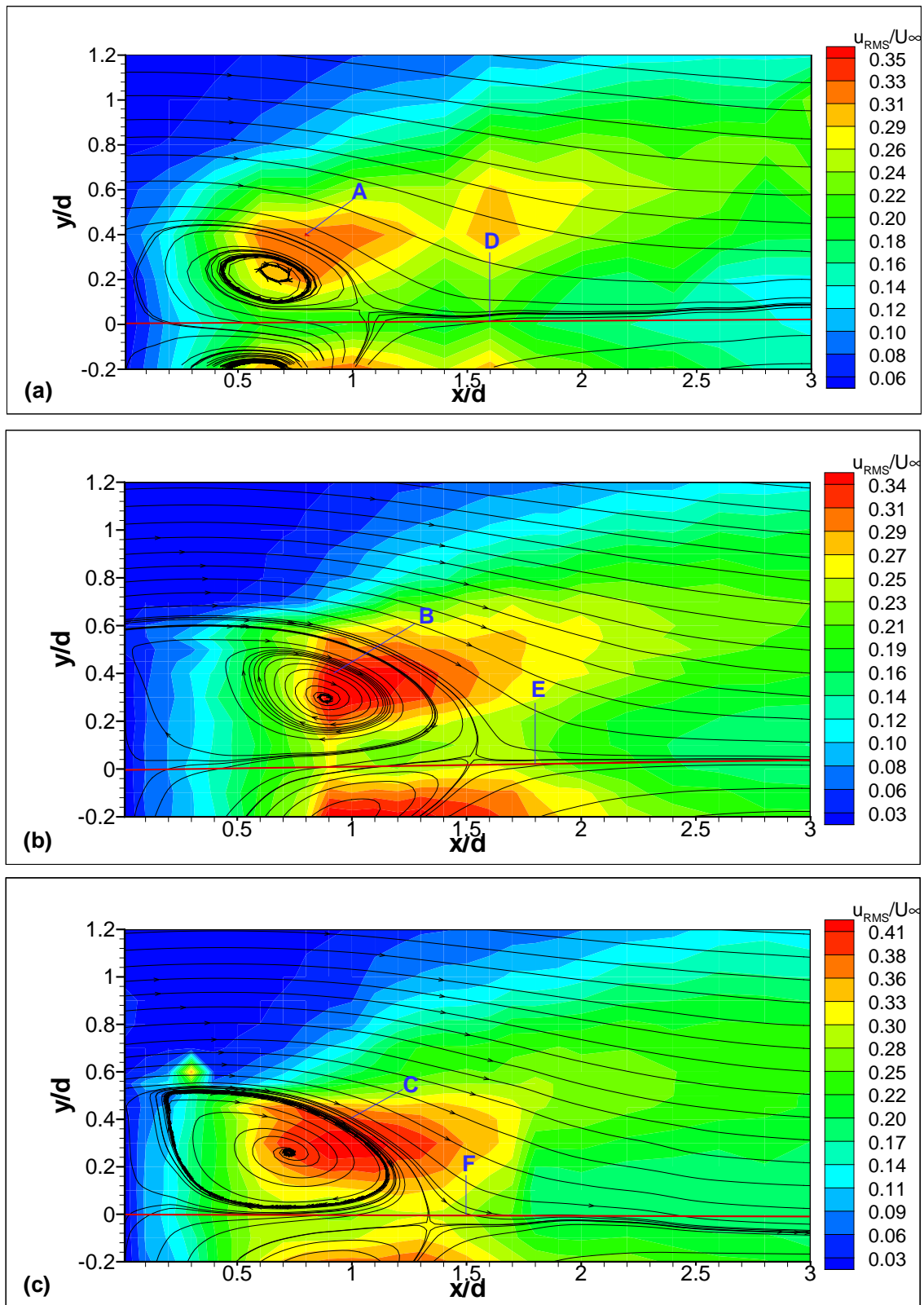


Figure 7. Longitudinal fluctuant velocity field with stream lines for the Reynolds numbers of (a) 0.6×10^3 (non-dimensional uncertainty of ± 0.01), (b) 1.7×10^3 (non-dimensional uncertainty of ± 0.01) and (c) 3.0×10^3 (non-dimensional uncertainty of ± 0.003).

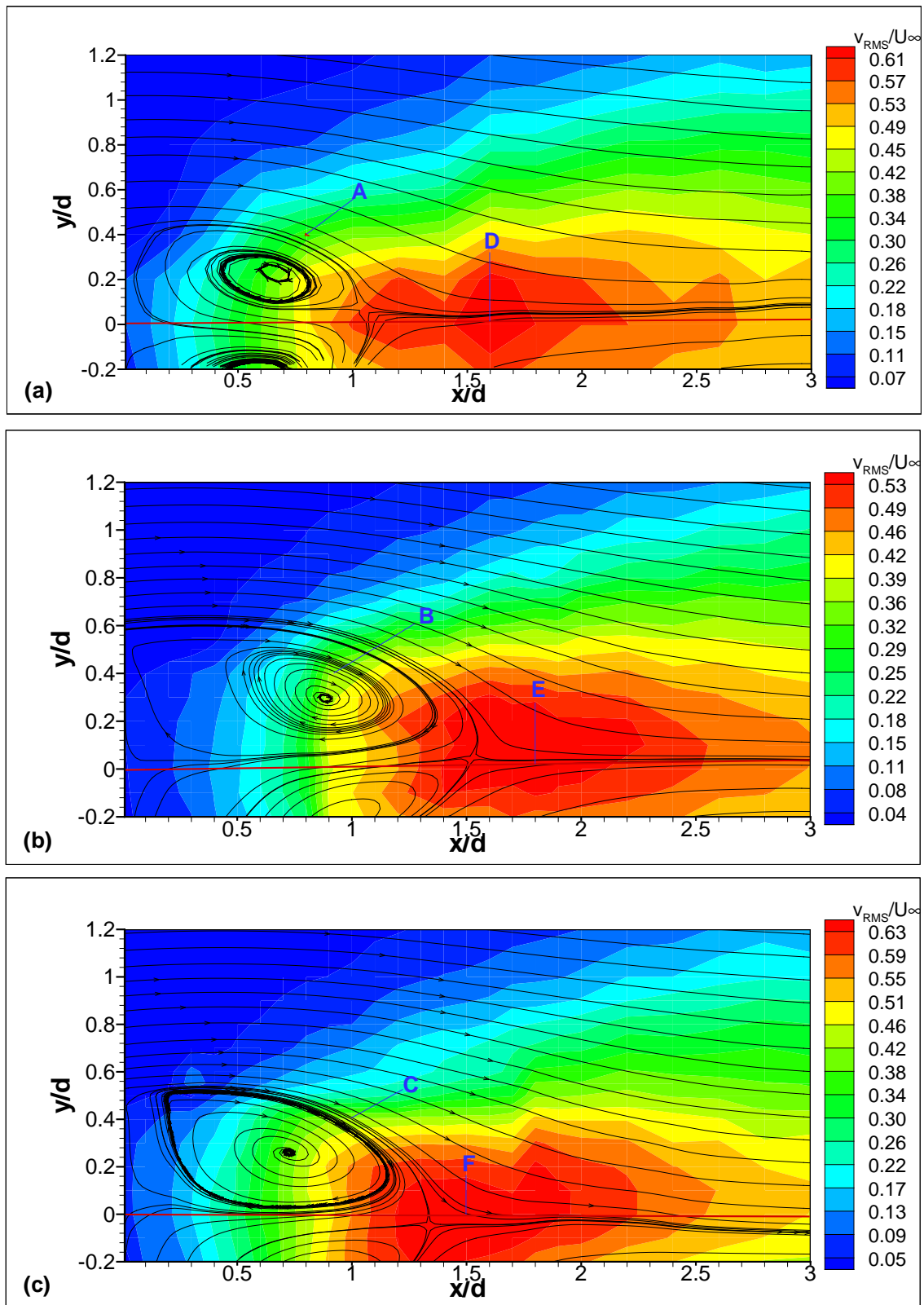


Figure 8. Transverse fluctuant velocity field with stream lines for the Reynolds numbers of (a) 0.6×10^3 (non-dimensional uncertainty of ± 0.02), (b) 1.7×10^3 (non-dimensional uncertainty of ± 0.01) and (c) 3.0×10^3 (non-dimensional uncertainty of ± 0.003).

Despite the mean vortex strength increment, and so the induced velocities, we can observe from the figure 7 that its maximum do not change so much with the Reynolds number variation. However there is a peculiar tendency on the formation region length (characterized by maximum u_{RMS} position), that in the first Re increment grows and diminishes in the second one. This shortening can be related to a faster shear layer rolling up due to the inertial force weakening, by the boundary layer thickness decrement, as can be observed from the Fig. 5.

From the figure 5 we can observe that the free shear layer gets thinner with the Reynolds number increment, and the vorticity becomes more concentrated, as said before. When the shear layer gets thinner the inertial force gets weaker and the vorticity concentrated makes the free layer roll up before.

But as explained before, due to the uncertainty associated to maximum fluctuant velocity positions, we cannot ensure that the maximum u_{RMS}/U_∞ position increases from $Re = 1.7 \times 10^3$ to $Re = 3.0 \times 10^3$. However from the streamlines shown in the figures above, we can observe the mean vortex decreasing.

From the figure 8 we can observe that the fluctuations maximums in the transversal direction do not change so much with the Reynolds number increasing. We can also observe the maximum v_{RMS} occur in the wake center line ($y = 0$). This results have the same u_{RMS} problem, however there is no uncertainty overlapping that can harm any conclusion, about its tendency. We can also observe that this fluctuation maximum has the same behavior of the mean vortex core, what can represent some correlation between them.

The results presented in this paper were not compared to any other due to the lack of reported results for this wedge model and wedges, in general, for such a Reynolds number.

5. Final Remarks

The measurements performed in this work presented a small uncertainty, reflecting the quality of employed methodology. The use of laser Doppler anemometry brings more possibilities for bluff bodies understanding, once it is able to separate the velocity fields in their mean and fluctuant components without disturbing the flow with its own presence. The equipment also makes low Reynolds number more reliable, because there is no calibration uncertainty associated to the measurement. The exception here is the vorticity field, which is affected by the traverse displacement uncertainty (0.1mm).

The results presented in this paper are of interest for *DNS* applications, mainly because of the fluctuant velocity and the mean vorticity fields at such a Reynolds number, however for the vorticity field reliable use an experimental setup improvement is required.

Despite the uncertainty for the maximum fluctuant velocity positions, the results present a good correlation among the flow parameters shown in the table 1, main for the x-direction length, X_N/d , X_{vr}/d and l_S/d . Although the good results obtained here these experiments can be done with a refined mesh at important points, such as the saddle point and maximum u_{RMS} , improving the results quality.

We can observe that the boundary layer thickness alters the near wake topology, imposing a back and forth movement to wake parameters, such as the mean core and saddle point positions. The mean core movement forward the base body is followed by a larger increment in the base pressure coefficient.

6. Acknowledgements

To Coordenação de Aperfeiçoamento de Pessoal de Nível Superior (CAPES) and to Fundação Casimiro Montenegro Filho, for supporting part of the resources used in this research. To all the staff of the Prof. K.L. Feng Aeronautical Engineering Laboratory. To FAPESP and EMBRAER for the financial support used to acquire the LDA equipment.

7. References

- Ahlborn, B.; Seto, M.L.; Noack, B.R., 2002, "On drag, strouhal number and vortex street structure" Fluid Dynamics Research, vol. 30, pp 379-399.
- Araújo, T.B. and Girardi, R.M., 2008, "Laser Doppler anemometry application for wedges near wake study", Proceedings of 12th Brazilian Congress of Thermal Engineering and Sciences, vol. 1, Belo Horizonte, Brazil.
- Araújo, T.B. and Girardi, R.M., 2009a, "Blockage Ratio Influence in 2-D Bluff Body Near Wake at Low Reynolds Number", Proceedings of 20th International Congress of Mechanical Engineering, Gramado, Brazil.
- Araújo, T.B. and Girardi, R.M., 2009b, "Separation Angle Influence in the Near Wake of 2-D Bluff Body", Proceedings of 20th International Congress of Mechanical Engineering, Gramado, Brazil.
- Bearman, P.W., 1965, "Investigation of flow behind a two-dimensional model with a blunt trailing edge and fitted with splitter plates", Journal of Fluid Mechanics, Vol.21, pp. 241-255.
- Fage, A. and Johansen, F.C., 1927, "On the flow of air behind an inclined flat plate of infinite span", Proc. Roy. Soc., vol. 116, pp.170-197.
- Girardi, R.M., Cavalieri A.V.G, Araújo, T.B., 2007, "Aerodynamic tests of the fuselage of ITA's unmanned aerial vehicle",

Proceedings of 19th International Congress of Mechanical Engineering, Brasilia, Brazil.

Glezer A. and Amitay, M. 2002, "Synthetic Jets", *Annu. Rev. Fluid Mech.*, Vol 34, pp 503-529.

Jensen, K. D., 2004, "Flow measurements", *J. of the Brazilian Soc. Mechanics Sciences and Engineering*, Vol.26, pp. 400-419.

Melling, A., 1997, "Tracer particles and seeding for particle image velocimetry", *Meas. Sci. Technol.* Vol.8, pp.1406-1416

Milne-Thomson, L., 1974, "Theoretical hydrodynamics", 5 ed., Mineola, N.Y. Dover.

Mittal, S., 2001, "Computation of three-dimensional flow past circular cylinder of low aspect ratio", *Physics of Fluids*, Vol.13, pp. 177-191.

Rathakrishnan, E., 1999, "Effect of splitter plate on bluff body drag", AIAA Journal Technical Report.

Roshko, A., 1954, "A New Hodograph for Free-streamline theory", NACA Technical Note 3168.

Sousa, F.L., 1993, "Influência da razão de bloqueio no escoamento plano sobre corpos rombudos", Msc Thesis - Instituto Tecnológico de Aeronáutica.

Tian, Q., Lowe, K.T., Simpson, R.L., 2007, "A three-velocity-component laser-doppler-velocimeter for measurements inside the linear compressor cascade", *Experiments in Fluids*, Vol. 43, pp. 487-499.

8. Responsibility notice

The author(s) is (are) the only responsible for the printed material included in this paper